ADVANCED ENGINEERING MATERIALS
www.aem-journal.com

Piezoelectric Drop-On-Demand Inkjet Printing of High-Viscosity Inks

*Roberto Bernasconi, Stefano Brovelli, Prisca Viviani, Marco Soldo, Domenico Giusti, and Luca Magagnin**

Drop-on-demand inkjet printing of highly viscous fluids represents a highly attractive emerging technology for advanced material deposition. The jetting of viscous inks, such as concentrated polymer solutions and nanoparticle suspensions, is a key enabling technology for many industrial applications, ranging from microelectronics to biomedicine and ceramics manufacturing. Currently available standard inkjet printers typically operate in a relatively narrow viscosity range (up to 16 mPa s), and alternative drop-on-demand printing techniques (such as laser-induced forward transfer) present limited industrial applicability. In this context, the development of a piezoelectric-driven printhead capable of jetting high-viscosity fluids is of great interest. Herein, a prototype of such a device is presented and its performance is evaluated using model fluids at increasing viscosities. Specifically, the dependence of emitted droplets' properties on jetting parameters is evaluated and linked to the physical characteristics of the system. In optimal conditions, piezoelectric jetting of solutions characterized by viscosities in excess of 200 cP is achieved. Finally, as an applicative example, the jetting of functional inks is attempted. A ZnO suspension and a poly(3,4-ethylenedioxythiophene) (PEDOT) based solution are successfully jetted to demonstrate the applicability of the developed printhead to the deposition of ceramic suspensions and concentrated polymer solutions.

1. Introduction

Inkjet printing (IJP) has been adopted as a material deposition technology in different fields, such as, electronics,[1] biology,[2] and biomedicine,[3] being a fully recognized flexible, scalable, and cost-effective technique.[4,5] In contrast to more traditional manufacturing techniques, IJP is a solution-based maskless additive technique, allowing minimum material waste combined with extreme precision in controlling the deposition of active material droplets in the picoliter range.[6–9] There are two main IJP modes of operation: the continuous inkjet printing (CIJ) and the drop-on-demand (DOD) system.[10] Despite CIJ being widely exploited in graphical applications, such as coding and marking, the great advantage of a DOD system over CIJ is the possibility to print smaller features (i.e. ≈20–50 μm vs ≈100 μm of CIJ) and that the ink droplet is ejected only when is needed, eliminating most of the complex structural parts present in CIJ.[11] Finally, CIJ systems involve a recycling system that can potentially cause the contamination of the ink itself.[12,13] Current DOD ink-printing technology works through various methods, such as thermal, electrostatic, piezoelectric (PZT), acoustic, and laser-assisted.[14–16] The active material is processed as a solution, i.e., ink, requiring specific physical properties to be framed in very restricted ranges of values to guarantee ink printability.[17] For example, the upper limit of viscosity for IJP is 20–40 mPa s.[18] This represents one of the major drawbacks of the DOD system, which shows severe limitations in ink printability.

A possible solution to reduce the viscosity is to increase the temperature. Despite being a very intuitive and simple method, some issues may arise when dealing with temperature-sensitive inks as their properties can be degraded beyond a certain temperature value. The need for low-viscosity inks poses many limitations because inks generally require high dilution to be processed. This translates to a reduction of the functional material content, resulting in the necessity of printing more layers to reach a certain target thickness. However, printing many layers can affect and lower the final resolution of the printed pattern. In addition to this issue, the necessity of keeping low the concentration of the functional material is a potential limiting factor for the formulation of inks capable of limiting the well-known coffee ring effect (CRE). The CRE is an extremely common defect defined as the progressive accumulation of nonvolatile material toward the edges, with a consequent depletion from the inner

R. Bernasconi, S. Brovelli, P. Viviani, L. Magagnin
Dipartimento di Chimica
Materiali e Ingegneria Chimica "Giulio Natta"
Via Mancinelli 7, 20131 Milano, Italy
E-mail: luca.magagnin@polimi.it

S. Brovelli, M. Soldo, D. Giusti
AMS Group
STMicroelectronics
Via Tolomeo 1, 20010 Cornaredo, Italy

The ORCID identification number(s) for the author(s) of this article can be found under https://doi.org/10.1002/adem.202100733.

DOI: 10.1002/adem.202100733

regions after solvent evaporation, driven by capillary fluxes toward the edges.[19,20]

Printing highly viscous inks through DOD systems remains an open challenge, which needs to be further studied, driven by the need of aforementioned issues and of printing fluids with nonlinear rheological behavior. Highly viscous polymers and colloidal or ceramic suspensions are an example. Moser and co-workers[21] demonstrated the possibility to consistently generate satellite-free viscous droplets (up to 200 mPas) on demand through laser actuation. By focusing a nanosecond laser pulse on a glass microcapillary, which acts as the nozzle of the DOD system, a shockwave is generated, resulting in a supersonic jet. Hague and co-workers[22] used a PZT-actuated jetting system to precisely jet materials of a wide range of viscosity, i.e., 20–100 000 mPa s. Laser-induced forward transfer (LIFT) is an alternative nozzle-free DOD technique. It enables to cover a wider selection of printable materials, such as for highly viscous suspensions, and to maintain high resolutions of the order of a few micrometers.[23] Zergioti and co-workers[24] were able to print fluids up to 1700 mPa s, corresponding to Z down to 0.03, demonstrating the possibility to print volumes as small as a few picoliters in a controllable way. Choi et al.[25] successfully printed a highly viscous copper paste using another promising technology for high-viscosity ink printing: electrohydrodynamic (EHD) jet printing. In the frame of DOD systems, a PZT printhead able to handle high viscosities would be beneficial in terms of ease of instrumentation and of the printable material selection range. In this framework, Condie et al.[26] have studied the jetting of highly viscous polymeric inks through the Xaar 1003 printhead, stating that fluids with significantly high viscosities (i.e., up to 100 cP) were printable.

Our work can be framed in this context. In particular, it aims at assessing and characterizing the performance of an innovative high-viscosity DOD printhead developed by ST Microelectronics. With respect to the technology developed by Xaar, the microfluidic system presented here is theoretically capable of jetting at significantly higher viscosities. To demonstrate this statement, the jetting behavior of various model solutions, at increasing viscosities, was investigated at ambient temperature. Specifically, model fluids were used to understand the macroscopic trends and their variations with the solution properties and the PZT actuator. In addition, two solutions of industrial interest were tested to provide an applicative perspective: a ZnO nanoparticle suspension and a high-grade PEDOT:PSS solution.

2. Results and Discussion

2.1. Fluids' Theoretical Printability

In inkjet printing, fluid properties such as viscosity (η) and surface tension (γ) have a strong influence on droplet formation.[27] It is possible to group such physical properties to define the so-called dimensionless Z number, which delineates the mechanics of drop formation (Equation (1)).

$$Z = \frac{\sqrt{d\rho\gamma}}{\eta} \tag{1}$$

d is a characteristic length (in general the nozzle diameter), ρ is the fluid density, γ is the surface tension, and η is the viscosity. Reis and Derby[28] defined $1 < Z < 10$ as a range where printability is optimal, while Jang et al. defined $4 < Z < 14$ as the optimal printability range.[29] The upper limit represents the conditions for generation of noncontrolled droplet ejection, i.e., satellites, which are smaller droplets separated from the head drop that can easily lose directionality.[8] This effect leads to a deterioration of the printing quality and precision. Lower values of Z, to which a high suspension viscosity corresponds, increase the difficulty of drop ejection because of the fluid viscous dissipation and pose significant issues related to nozzle clogging.[12,30] The main physical properties of the model fluids, relevant for inkjet solutions, are shown in **Table 1**. The values are calculated from the literature at 25 °C and for a characteristic length (nozzle diameter) of 40 μm. The composition is expressed as a volume fraction of the solute (ethylene glycol [EG] or glycerine [GLY]). Generally, by increasing the viscosity, surface tension, and density, the drop ejection requires more energy. In contrast, a higher speed of sound in the ink decreases the loss of energy of pressure waves traveling in the printhead channel and leads to a more efficient energy transfer to the drop. It is also important to point out that both water/EG and water/GLY mixtures exhibit a Newtonian behavior, with a viscosity that is independent of the shear rate applied.[31]

As Z decreases (i.e., viscosity increases), the drop ejection is expected to be more and more difficult and, after a certain range, impossible. The transition between different working zones, characterized by satellites, perfect drops, and viscous dissipation, is gradual and depends not only on the Z values but also on the geometry and design of the printhead system. Indeed, for the very same ink, a system in which pressure waves, generated by the PZT membrane, are well controlled and amplified increases the energy transferred to the fluid and thus the possibility to eject more viscous inks.

2.2. Model fluids—Effect of Printhead Geometry

Keeping in mind these introductory considerations, the printhead hereby developed has been tested in two geometrical configurations, with two PZT compositions and at increasing ink viscosity. Initially, the effect of the geometry of the jetting chamber and of the nozzles was evaluated. For the same printhead material PZT_A, two printhead geometries and designs were compared: PD_A and PD_B. The respective geometrical features are reported in Table 1. As previously mentioned, these die designs support ink recirculation. This is particularly useful when dealing with ceramic-based inks with nano-sized particles.

Table 1. Physical properties of the fluids used and the corresponding Z values.

Fluid	ID	Composition [φ]	Viscosity [cP]	Surface tension [N m^{-1}]	Density [kg m^{-3}]	Speed of sound [m s^{-1}]	Z
H_2O/EG	EG10	0.865	10	0.05117	1100.50	1668.08	4.77
H_2O/GLY	GLY100	0.839	100	0.06485	1223.18	1907.70	0.56
H_2O/GLY	GLY200	0.897	200	0.06403	1236.21	1918.17	0.28
H_2O/GLY	GLY250	0.9145	250	0.06377	1240.06	1920.29	0.22
H_2O/GLY	GLY300	0.9275	300	0.06357	1242.88	1921.66	0.19

Due to a pressure difference applied at the inlets, the ink is not static but in constant motion. This helps avoiding phase separation and limiting clogging issues at the nozzles. Newtonian model fluids, specifically EG10 and GLY100, were considered to test the different printhead designs. Physical properties of the solutions are reported in Table 1. The EG-based solution (EG10) has a viscosity of 10 cP, a surface tension of 56 mN m^{-1}, and a speed of sound of 1670 m s^{-1}. The glycerin-based solution (GLY100) has a viscosity of 100 cP, a surface tension of 66 mN m^{-1}, and a speed of sound of 1970 m s^{-1}. Typical IJP viscosities are comprised between a few centipoises and 20 cP, with solutions close to the upper limit being hardly printable. A viscosity of 100 cP is far from the ideal range of printable IJP viscosities, so it could give an idea of the printhead effectiveness in jetting highly viscous solutions. Every printed solution was characterized by considering the drop kinetic energy, velocity, and volume by varying the pulse width upon a fixed voltage. **Figure 1** shows the results obtained for the EG10 solution: kinetic energy versus pulse width up to the onset satellites voltage (a), kinetic energy versus pulse width beyond the onset satellites voltage (b), drop velocity versus pulse width up to the onset satellite voltage (c), drop velocity versus pulse beyond the onset satellites voltage (d), drop volume versus pulse width up to the onset satellites voltage (e), and drop volume versus pulse width beyond the onset satellites voltage (f). EG10 was jetted exploiting the printhead design PD_A.

The curves obtained by varying the applied voltage up to the onset satellite voltage followed a nonmonotonic trend. At first, an increase of pulse width corresponded to an increase of kinetic energy, volume, and velocity. After a specific pulse width threshold, a decrease of such quantities was obtained. This aspect allowed us to identify an optimal pulse width (OPW) and an optimal voltage (OV), corresponding to 2.1–2.2 μs and 42 V, respectively. In correspondence of such values, the best performance in terms of kinetic energy, drop velocity, and volume was achieved. A kinetic energy of 150 pJ, a drop velocity of 4.3 m s^{-1}, and a drop volume of 13.5 pL were obtained. However, the head drop velocity was under the lower velocity limit for graphic printing, generally set at 5 m s^{-1} in the industry.[32] For values of voltage lower than 42 V, no satellite formation was observed. For voltage values greater than 42 V, onset of satellites was achieved. Due to the presence of the satellites, curves ceased following the ideal trend. Since the head drop split into multiple secondary drops, the volume decreased and lighter drops were not accelerated but rather slowed down, lowering the kinetic energy and velocity.

The appearance of satellites at a well-defined voltage can be explained by considering the physics of the fluid during ejection from the nozzle. Higher voltages correspond to higher speeds of the droplet (Figure 1c,d). During emission, each droplet maintains a ligament that prolongs from the main body of the droplet itself toward the nozzle.[33] Such a ligament, according to the properties of the ink (viscosity, surface tension) or the speed of the droplet, can undergo two competitive phenomena: recoil into the main drop or pinch off in proximity of the main drop.[34] In the first case, the material present in the ligament is successfully resorbed into the main droplet and no satellites form. In the second case, the ligament separates from the main drop and coalesces under the influence of surface tension into a satellite. At constant physical properties of the ink, the main factor influencing the behavior of the ligament is the speed of the main droplet. When the latter is high, the fluid does not have the time to recoil into the main droplet and pinch off occurs. In other words,
to avoid satellite formation according to the treatise by Marangoni et al.[34] the ratio between the characteristic time for pinch off and for recoil must be higher than 1.

Noteworthy is to consider the drop volume behavior trend. In correspondence of specific pulse width values, a decrease in volume was observed (as satellites were generated). Still, it was possible to reconstruct the ideal volume behavior in absence of satellites. **Figure 2**a shows the frequency response of the PD_A geometry, in terms of kinetic energy. Figure S3 and S4, Supporting Information, report the corresponding responses in terms of drop speed and volume, respectively.

A typical constructive/destructive interference pattern was observed. The maximum energy transfer to the liquid and efficiency were achieved in correspondence or in the vicinity of a peak, namely, in correspondence of the Helmotz frequency. By considering the OPW previously defined, it was found that the main resonant frequency for the fluid-printhead system lies between 227 and 238 kHz. This result is in good agreement with what is predicted by considering the known acoustic law for the Helmotz frequency (Equation (2)).

$$f_H = (2 \times OPW)^{-1} \tag{2}$$

In addition, good accordance was also found with the other peaks, specifically for $f_H/2$ (116 kHz), $f_H/3$ (75 kHz), and $f_H/4$ (55 kHz) peaks. The frequency response interruption between 130 and 160 kHz is due to an unstable firing condition of the system, in which the selection of the head drop to analyze was problematic. The frequency response in terms of kinetic energy of the PD_B was analyzed as well and compared with the behavior of the PD_A geometry (Figure S5, Supporting Information). The two designs present a comparable behavior, which is a logical consequence of their similar geometries. Figure 2b highlights the visual appearance of the droplets obtained at different jetting frequencies, namely, 100, 150, 230, and 275 kHz. Noteworthy is to mention how, at 150 kHz, a nonuniform drop generation is achieved, coinciding with the empty interval in the kinetic energy versus frequency.

Afterward, the GLY100 solution was analyzed to understand the printability behavior of a high-viscosity ink. **Figure 3** shows the results obtained for the 100 cP glycerin solution: kinetic energy versus pulse width up to the onset satellite voltage (a), kinetic energy versus pulse width beyond the onset satellite voltage (b), drop velocity versus pulse width up to the onset satellite voltage (c), drop velocity versus pulse width beyond the onset satellite voltage (d), drop volume versus pulse width up to the onset satellite voltage (e), and drop volume versus pulse width beyond the onset satellites voltage (f). GLY100 was jetted, in this case, exploiting the printhead design PD_A.

In analogy with EG10, the curves obtained by varying the applied voltage up to the onset satellite voltage followed a nonmonotonic trend. At first, an increase of pulse width corresponded to an increase of volume and velocity. After the OPW, a decrease of such quantities was observed. This aspect allowed us to identify the OPW and the OV, corresponding to

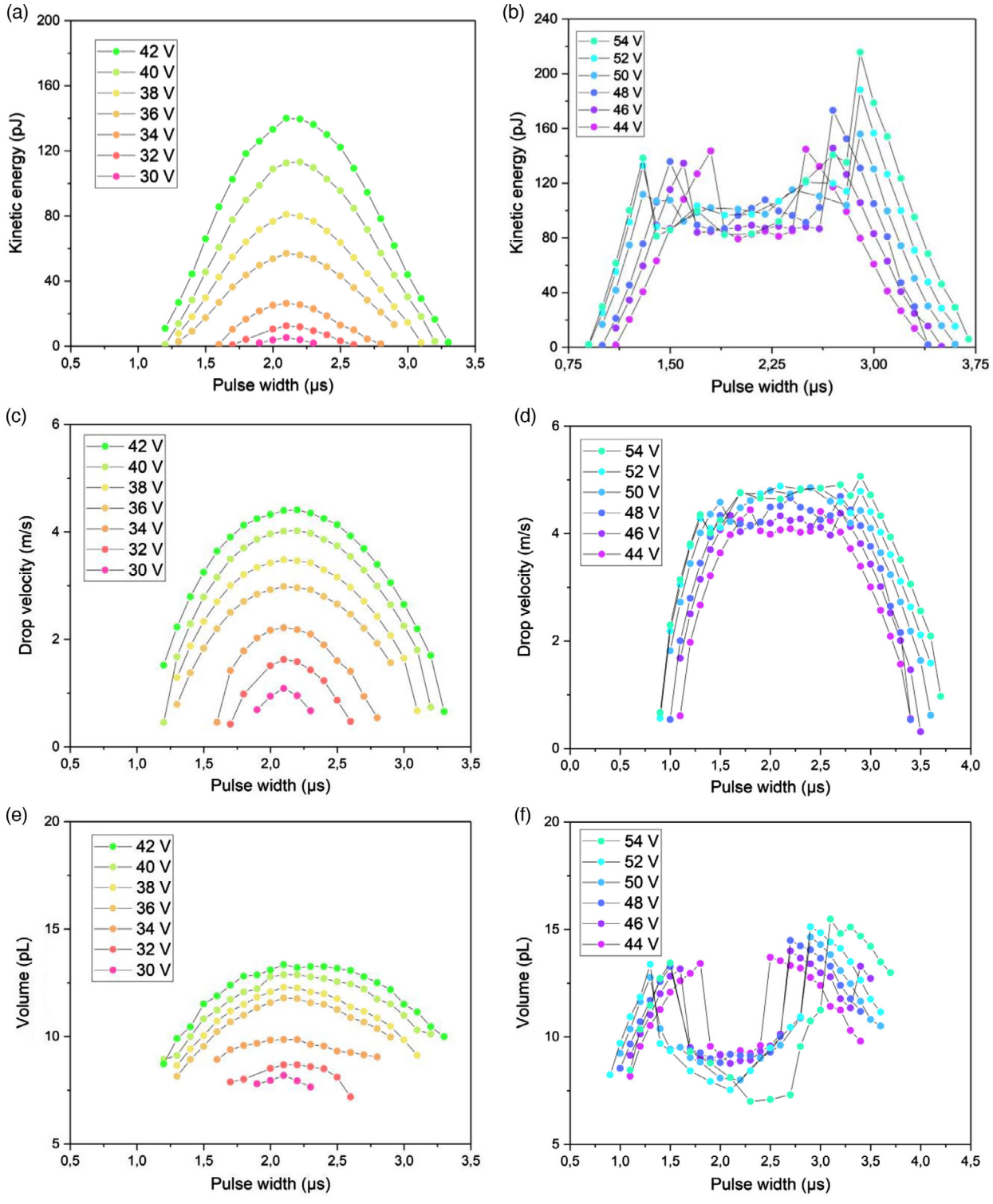

Figure 1. EG10 solution jetted through a PD_A printhead design featuring PZT_A material versus pulse width variation: a) kinetic energy by varying the applied tension up to the onset satellite voltage, b) kinetic energy by varying the applied tension beyond the onset satellite voltage (during satellites ejection), c) drop velocity by varying the applied tension up to the onset satellite voltage, d) drop velocity by varying the applied tension beyond the onset satellite voltage (during satellites ejection), e) drop volume by varying the applied tension up to the onset satellite voltage, and f) drop volume by varying the applied tension beyond the onset satellite voltage (during satellites ejection).

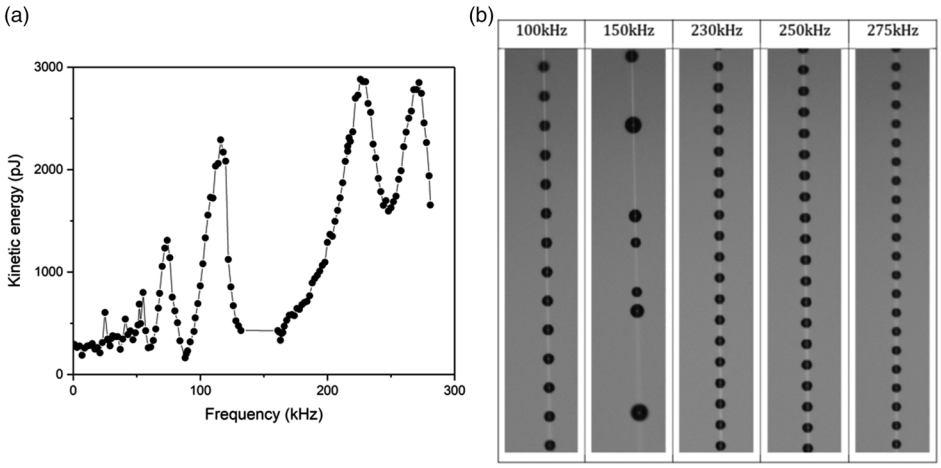

Figure 2. a) Frequency characterization of the PD_A design, in terms of kinetic energy, and b) visual appearance of emitted droplets versus jetting frequency.

2.1 μs and 38 V respectively. In correspondence with such values, the best performance in terms of kinetic energy, drop velocity, and volume was achieved. A kinetic energy of 850 pJ, a drop velocity of 8 m s^{-1}, and a drop volume of 24 pL were obtained. By comparing the collected results for the two solutions, EG10 and GLY100, it is possible to observe that the high-viscosity solution was able to provide higher values of velocity under optimal conditions in terms of OPW and OV. Although at first the opposite would be expected, because the glycerin solution should be dissipating more energy and thus be harder to jet, the glycerin solution has a higher speed of sound compared with the one of the EG mixture, 1930 and 1670 m s^{-1} respectively. This leads to the sound waves traveling in a more efficient way through the acoustic channel, thus encountering lower losses and dissipations. Regarding the volume profile, by increasing the viscosity of the solution more fluid is drawn outside the nozzle when a drop is ejected, resulting in a larger drop. This phenomenon is enhanced by the higher surface tension of the GLY solution. The base voltage at which the system starts to jet increases by increasing the ink viscosity. This is intuitive, considering that a higher-viscosity ink requires a higher PZT deflection to be jetted. In addition, the onset satellite voltage increases as the solution viscosity increases. Jetting of a 200 cP solution was not achieved with the design PD_A.

Figure S6, Supporting Information, shows the results obtained during the jetting for the 10 cP ethylene glycol solution (EG10), exploiting the printhead design PD_B and the material PZT_A: kinetic energy versus pulse width up to the onset satellite voltage (a), kinetic energy versus pulse width beyond the onset satellite voltage (b), drop velocity versus pulse width up to the onset satellite voltage (c), drop velocity versus pulse width beyond the onset satellite voltage (d), drop volume versus pulse width up to the onset satellites voltage (e), and drop volume versus pulse width beyond the onset satellite voltage (f). Once again, the curves obtained by varying the applied voltage up to the onset satellite voltage followed a nonmonotonic trend. It was possible to identify an OPW and an OV, corresponding to 2.1 μs and 32 V, respectively. Under such conditions, a kinetic energy of 80 pJ, a drop velocity of 3.8 m s^{-1}, and a drop volume of 9 pL were obtained. As previously mentioned, the velocity is under the commercial printing lower speed limit. However, despite the volume being rather small, this can fit applications in which precision is required. Figure S7, Supporting Information, shows the results obtained for the 100 cP glycerol solution (GLY100): kinetic energy versus pulse width up to the onset satellites voltage (a), kinetic energy versus pulse width beyond the onset satellite voltage (b), drop velocity versus pulse width up to the onset satellite voltage (c), drop volume versus pulse width up to the onset satellite voltage (d), drop volume versus pulse width up to the onset satellite voltage (e), and drop volume versus pulse width beyond the onset satellite voltage (f). Such results were collected exploiting the printhead design PD_B.

Similarly to the previous cases, the curves obtained by varying the applied voltage up to the onset satellites voltage followed a nonmonotonic trend. However, the bell-shaped curves were found to be less defined. Figure S8, Supporting Information, shows the typical jetting behavior observed beyond the onset of satellites. Again, it was possible to identify an OPW and an OV, corresponding to 2.3 μs and 38 V, respectively. Under such conditions, a kinetic energy of 600 pJ, a drop velocity of 8 m s^{-1}, and a drop volume of 20 pL were observed. It was also possible to observe that the base voltage at which the system started to jet increased with solution viscosity, i.e., 26 V for EG10 solution and 32 V for GLY100 solution. This effect is somewhat expectable as more viscous solutions dissipate more energy and are thus more difficult to move through the nozzle. The same trend was found in the satellite onset voltage. An increase in drop velocity and volume was observed as the viscosity of the solution increased, as previously indicated. In conclusion, by comparing the obtained results for both geometries, the design PD_A provides greater volumes under the same viscosity conditions. This aspect is ascribable to the bigger geometrical features of the design PD_A, such as for the chamber width and nozzle diameter, so the system collects more material in correspondence of the chamber and, eventually, at the nozzle. In turn, the PZT membrane of the PD_B design is stiffer, leading to higher drop velocities for the same driving pulse but, due to smaller geometrical features, lower volumes.

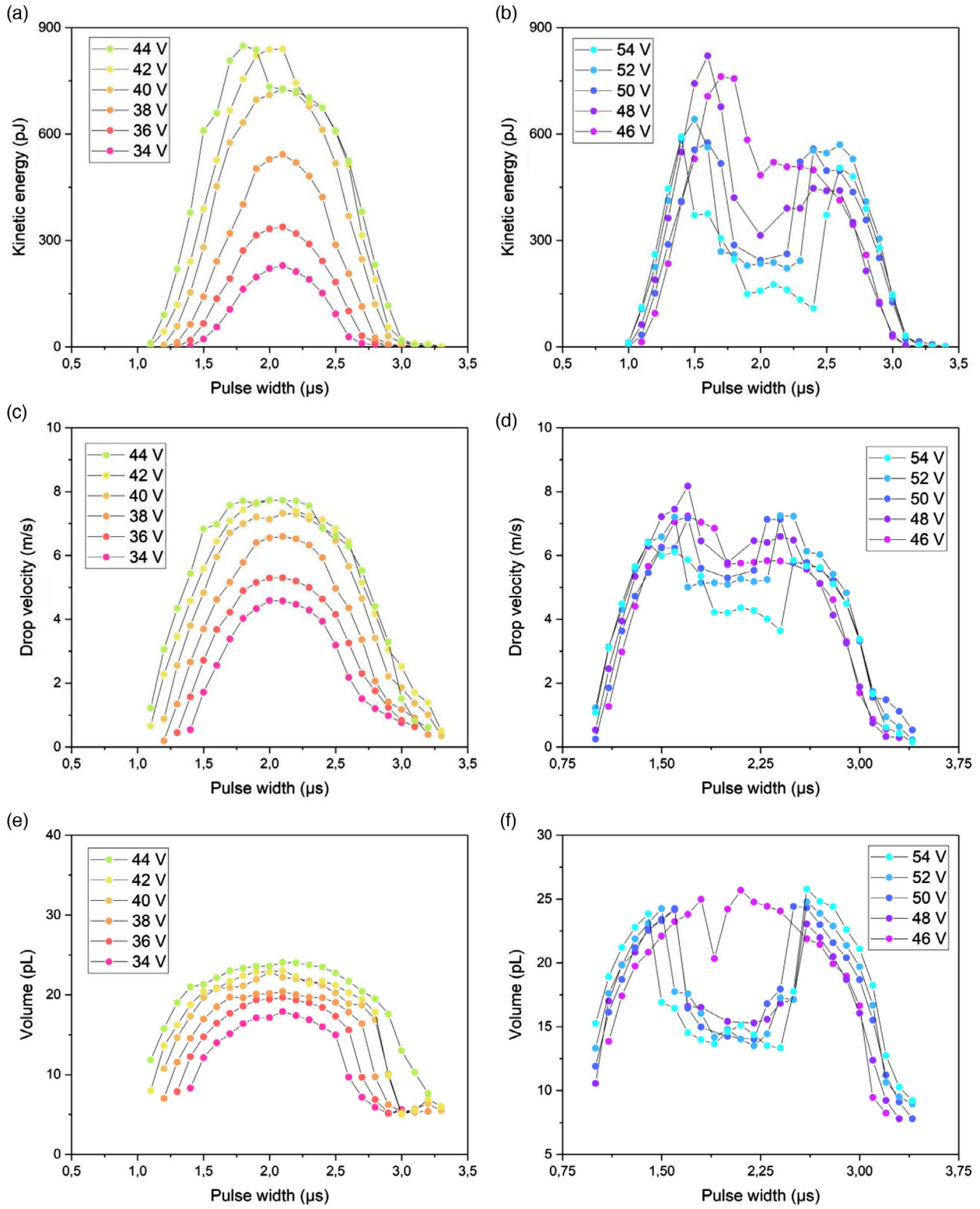

Figure 3. GLY100 solution jetted through a PD_A printhead design featuring PZT_A material versus pulse width variation: a) kinetic energy by varying the applied tension up to the onset satellite voltage, b) kinetic energy by varying the applied tension beyond the onset satellite voltage (during satellites ejection), c) drop velocity by varying the applied tension up to the onset satellite voltage, d) drop velocity by varying the applied tension beyond the onset satellite voltage (during satellites ejection), e) drop volume by varying the applied tension up to the onset satellite voltage, and f) drop volume by varying the applied tension beyond the onset satellite voltage (during satellite ejection).

2.3. Model Fluids—Effect of PZT Materials

Apart from geometry, the effect of two different PZT materials was investigated at increasing viscosities. For the same printhead design PD_B, two PZT materials were compared: PZT_A and PZT_B. The same model fluids were considered to test the different PZT material printheads, specifically EG10 and GLY100, with the same physical properties reported in Table 1. In addition, as the PD_B geometry allowed jetting of solutions with viscosity higher than 100 cP, a 200 cP water/GLY mixture was tested as well (GLY200). Consequently, the tested viscosities ranged between 10 and 200 cP. This range was determined according to the jetting ability of the printhead, which was linked to the geometry and to the specific PZT material. Results related to the EG and GLY100 solutions jetted through a PD_B printhead design featuring a PZT_A material were previously reported in Figure S6 and S7. These results are now compared to those obtained when such solutions are jetted through a PD_B printhead design featuring a PZT_B material. Figure S9, Supporting Information, shows the trends observed for the EG10 solution jetted with PZT_B material and PD_B geometry: kinetic energy versus pulse width up to the onset satellite voltage (a), kinetic energy versus pulse width beyond the onset satellite voltage (b), drop velocity versus pulse width up to the onset satellite voltage (c), drop velocity versus pulse width beyond the onset satellite voltage (d), drop volume versus pulse width up to the onset satellite voltage (e), and drop volume versus pulse width beyond the onset satellite voltage (f). The curves obtained by varying the applied voltage up to the onset satellite voltage followed the same nonmonotonic trend, even though after the satellite onset the original bell-like shape was lost. It was still possible to identify an OPW and an OV, corresponding to 2.1 μs and 34 V, respectively. Under these optimal conditions, a kinetic energy of 800 pJ, a drop velocity of 11 m s^{-1}, and a drop volume of 12 pL were achieved. Satellites were detected for voltages greater than 34 V.

Figure 4 refers to the results related to the jetting of the GLY100 solution with the PZT_B material and the PD_B geometry: kinetic energy versus pulse width up to the onset satellite voltage (a), kinetic energy versus pulse width beyond the onset satellite voltage (b), drop velocity versus pulse width up to the onset satellite voltage (c), drop velocity versus pulse width beyond the onset satellite voltage (d), drop volume versus pulse width up to the onset satellite voltage (e), and drop volume versus pulse width beyond the onset satellite voltage (f).

It was possible to identify an OPW and an OV, corresponding to 2.1 μs and 38 V, respectively. Under these optimal conditions, a kinetic energy of 950 pJ, a drop velocity of 10 m s^{-1}, and a drop volume of 17 pL were achieved. Satellites were detected for voltages greater than 38 V. Unlike the geometry PD_A with PZT_A, it was possible to jet highly viscous GLY inks with the printhead equipped with the PZT_B material and characterized by the PD_B geometry. **Figure 5** shows the results obtained from the jetting of a 200 cP GLY ink (GLY200): kinetic energy versus pulse width up to the onset satellite voltage, kinetic energy versus pulse width beyond the onset satellite voltage, drop velocity versus pulse width up to the onset satellite voltage (c), drop velocity versus pulse width beyond the onset satellite voltage (d), drop volume versus pulse width up to the onset satellite voltage (e), and drop volume versus pulse width beyond the onset satellite voltage (f).

The OPW and OV corresponded to 2.2 μs and 49 V, respectively. Under these optimal conditions, a kinetic energy of 430 pJ, a drop velocity of 6 m s^{-1}, and a drop volume of 20 pL were achieved. Satellites were detected for voltages greater than 51 V. **Figure 6** shows the jetted droplets in different conditions.

As indicated by the graphs visible in Figure 5, the drop volume visibly increased moving to higher potentials (from 43 to 58 V). The same consideration is valid for the drop velocity and, consequently, for kinetic energy. When jetting in out-of-resonance conditions (6.1 μs as PW), bigger but slower drops were observed.

By comparing the three solutions tested with PZT_B and PD_B, there is a good accordance between the increase of viscosity and the effects observed. In particular, by plotting the different quantities with respect to the voltage applied, viscosity effects can be clearly evidenced (**Figure 7**). Figure 7a refers to the jetting of the EG10 solution with PZT_B and PD_B. In general, the observed response in terms of kinetic energy of the droplets to different voltages can be divided into three zones. In zone I, which extends from the base voltage at which the system starts to jet to zone II, the kinetic energy is very low and it increases slowly with voltage. Here, the energy transferred from the actuator to the fluid in the jetting chamber is mostly used to overcome surface tension in correspondence with the nozzle. Consequently, the final energy of the resulting droplets is relatively low. In zone II, which extends between zone I and the onset of satellite formation, the energy of the actuator efficiently transfers to the fluid, resulting in a linear relationship between the voltage applied and the kinetic energy of the droplets. The displacement of the actuator (and consequently the force that it is able to apply) scales linearly with the voltage and the kinetic energy of the droplets follows the same trend. In zone III, the system starts to generate satellite droplets and the kinetic energy starts following an irregular path. The data obtained for GLY100 and GLY200 were plotted together with EG10, yielding Figure 7b–d.

All the kinetic energy curves present the same structures, characterized by the three zones I, II, and III. The base voltage at which the system starts to jet increases with the viscosity, i.e., 22 V for the EG10 solution, 28 V for the GLY100 solution, and 33 V for the GLY200 solution. In addition, the same trend was observed looking at the onset of satellites, i.e., 34 V for EG10 solution, 38 V for GLY100 solution, and 51 V for GLY200.

All these aspects are expected considering the data reported in Table 1. As previously mentioned, a decrease of Z values below 1 is expected to make droplet ejection increasingly difficult (and, at a certain point, impossible). The effect can be explained considering that a higher viscosity of the solution is more demanding in terms of the required energy to jet the droplets. Indeed, by comparing the kinetic energies of the three solutions, a decrease of kinetic energy between the 10 cP EG and the 200 cP GLY ink is observed and justified considering that part of the transferred energy to the fluid is dissipated due to the higher viscosity of the ink. This also explains why the drop velocity decreases following a monotonic trend by increasing the viscosity, for the same driving conditions. A different trend is shown by the drop volume, which generally increases along with viscosity, because more fluid is drawn from the nozzle. By looking at Figure 7,

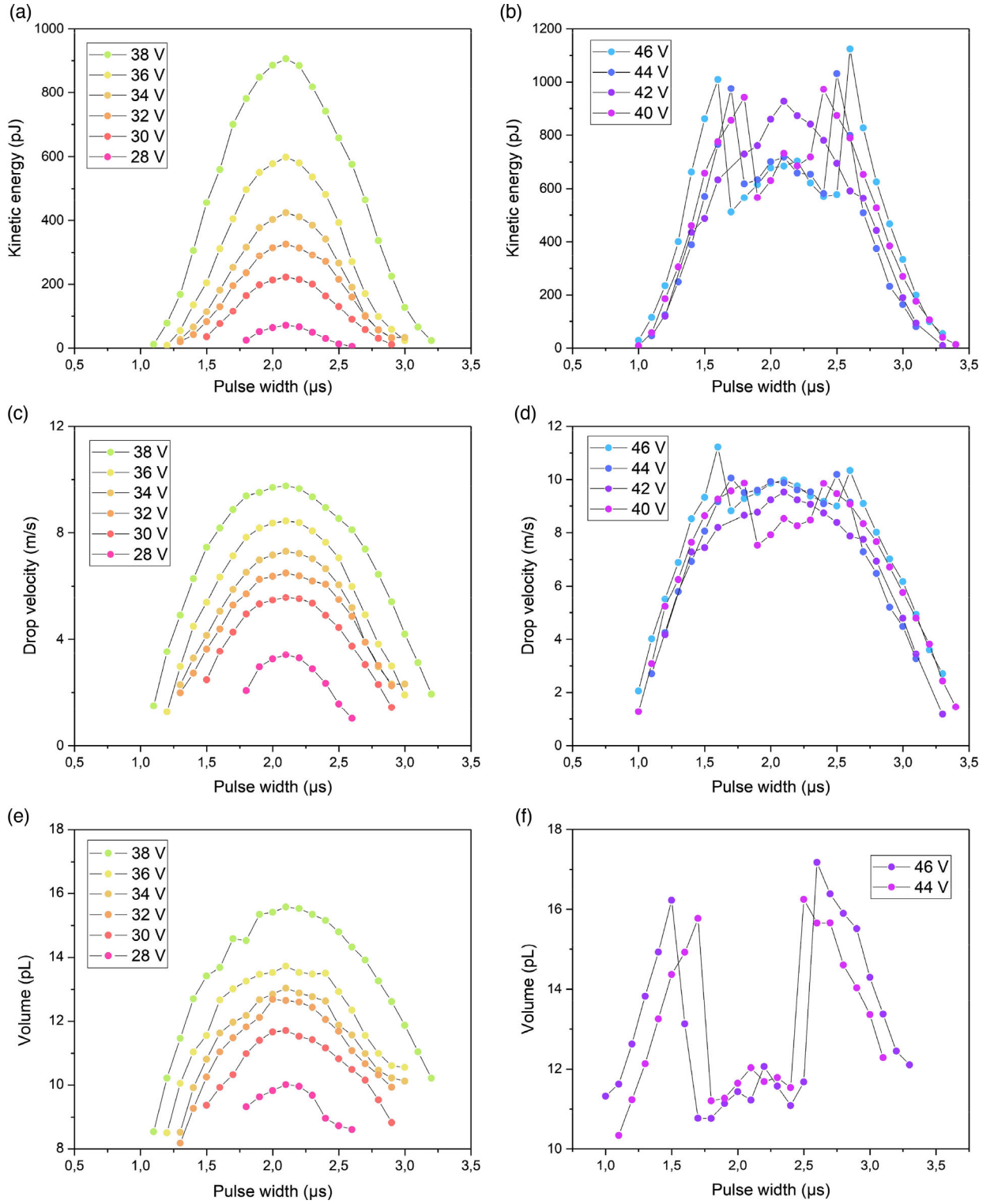

Figure 4. GLY100 solution jetted through a PD_B printhead design featuring PZT_B material versus pulse width variation: a) kinetic energy by varying the applied tension up to the onset satellite voltage, b) kinetic energy by varying the applied tension beyond the onset satellite voltage (during satellites ejection), c) drop velocity by varying the applied tension up to the onset satellite voltage, d) drop velocity by varying the applied tension beyond the onset satellite voltage (during satellite ejection), e) drop volume by varying the applied tension up to the onset satellite voltage, and f) drop volume by varying the applied tension beyond the onset satellite voltage (during satellite ejection).

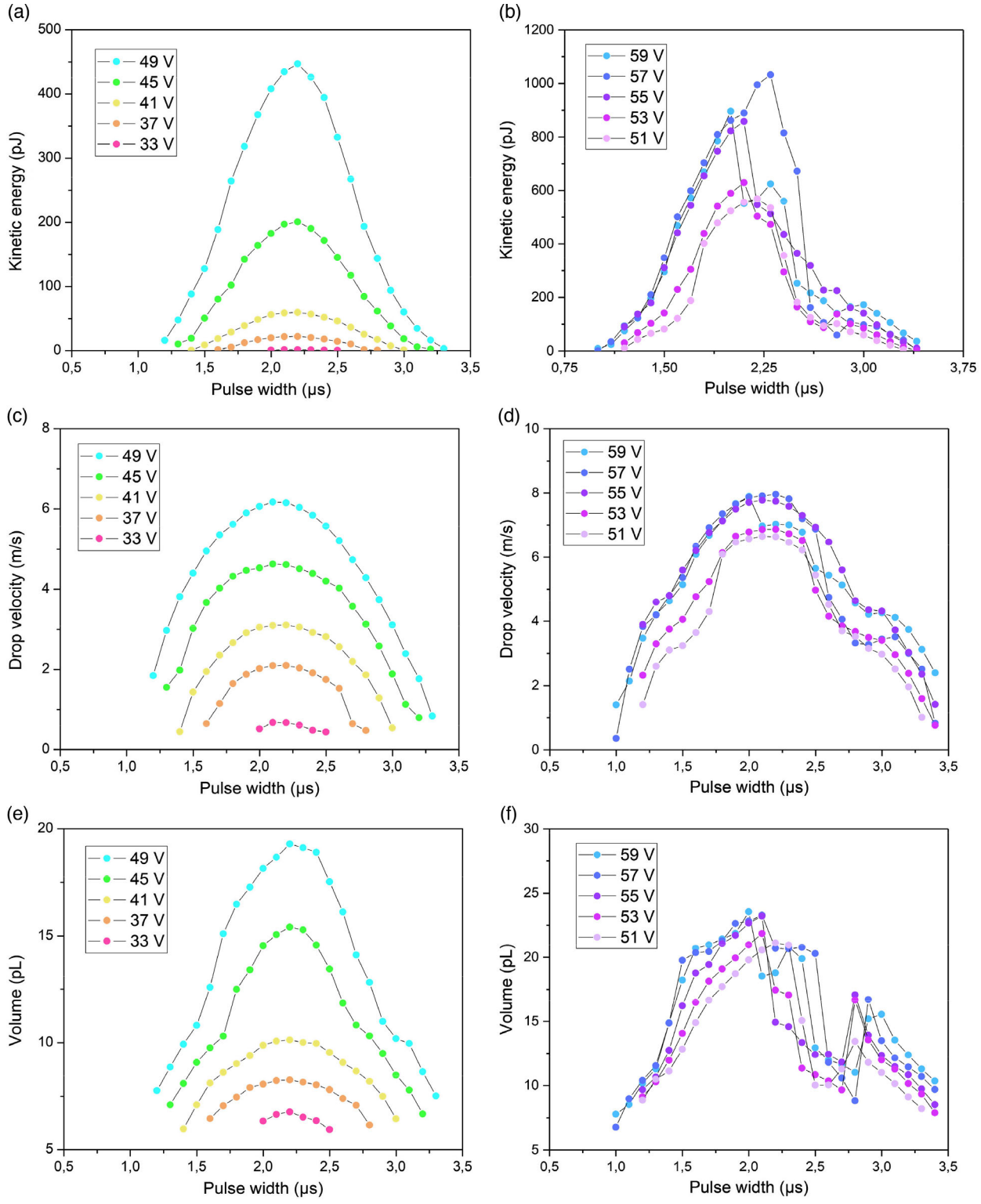

Figure 5. GLY200 solution jetted through a PD_B printhead design featuring PZT_B material versus pulse width variation: a) kinetic energy by varying the applied tension up to the onset satellites voltage, b) kinetic energy by varying the applied tension beyond the onset satellite voltage (during satellites ejection), c) drop velocity by varying the applied tension up to the onset satellite voltage, d) drop velocity by varying the applied tension beyond the onset satellite voltage (during satellites ejection), e) drop volume by varying the applied tension up to the onset satellite voltage, and f) drop volume by varying the applied tension beyond the onset satellite voltage (during satellites ejection).

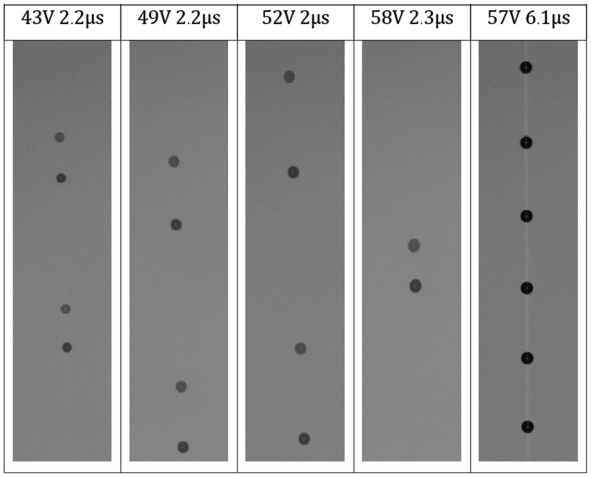

Figure 6. GLY200 jetting in different conditions through a PD_B printhead design featuring PZT_B material.

the general tendency observed is the following: when viscosity increases, jetted droplets travel at decreasing maximum velocities in front of increasing volumes. These two effects tend to counterbalance, yielding comparable levels of maximum achievable kinetic energy.

Finally, also, the two different PZT materials manifest their influence on the achieved printhead performance in terms of printing ability. Indeed, a 200 cP ink solution could be jetted only with the PZT_B material. The PZT_A material was considerably less performant compared to the PZT_B material, its composition being out of the MBP. This aspect is ascribed to the different final material compositions. It is well known that PZT materials exhibit increased PZT response over a specific compositional range, i.e., the morphotropic phase boundary composition. In correspondence with this range, a composition-induced structural phase transition occurs, known as morphotropic phase transition, where multiple phases coexist at room temperature.[35,36] The better performance of the PZT_B material is also reflected in the minimum driving voltage needed for jetting, being more sensitive to the applied electric field.

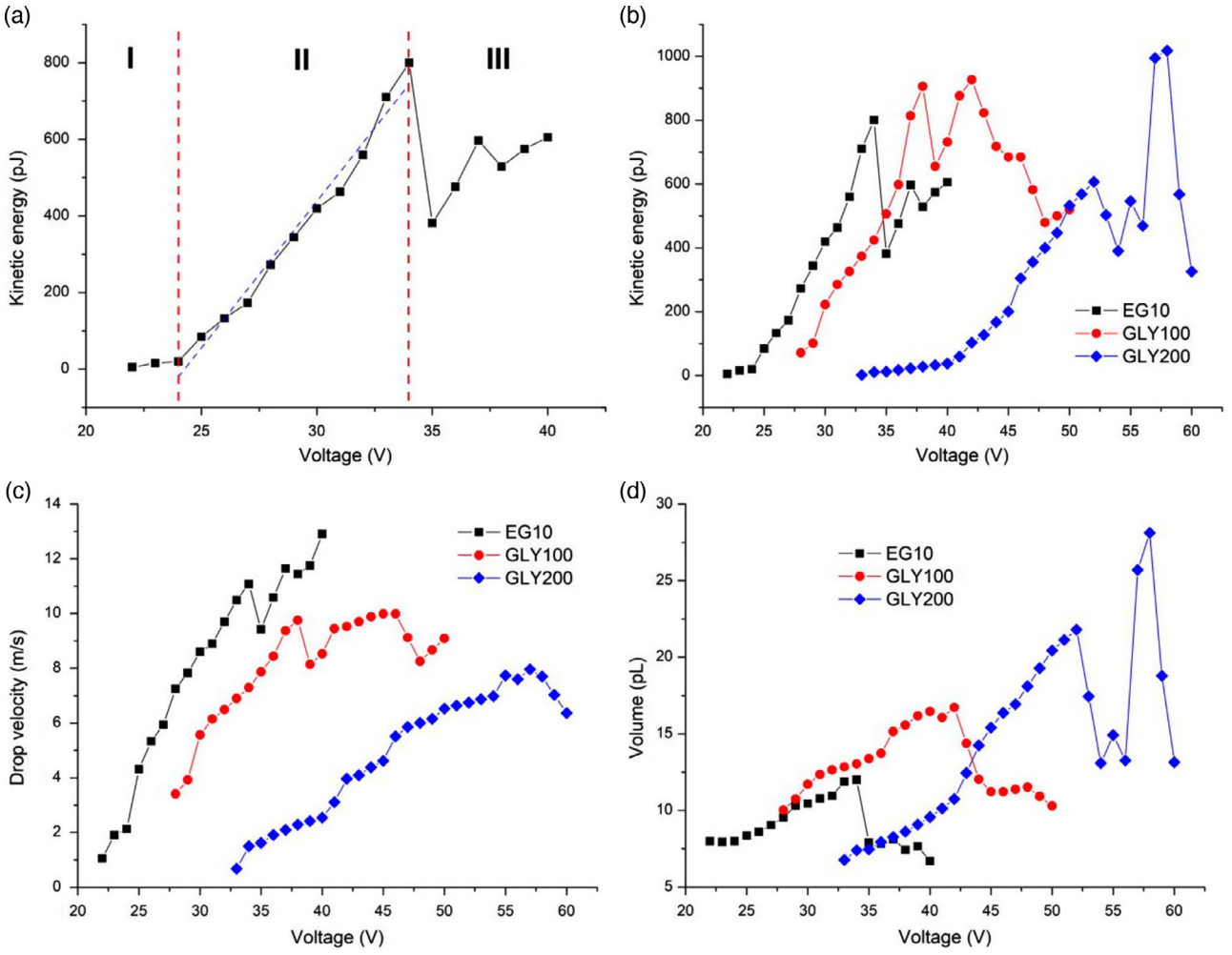

Figure 7. a) Kinetic energy versus applied voltage for EG10 jetting through a PD_B printhead design featuring PZT_B material, b) kinetic energy versus applied voltage for the three model fluids, c) drop velocity versus applied voltage for the model fluids, and d) drop volume versus applied voltage for the three model fluids.

Following the tests with the 200 cP model fluid, the system was still in a good state, without visible failures. Consequently, the upper limit of viscosity was explored using 250 cP (GLY250) and 300 cP (GLY300) solutions. In both cases and after several trials, even at high voltages close to the maximum for the class-D audio amplifier, jetting was not achieved, even in unstable conditions. Reasonably, the jetting onset moved to potentials too high for the setup used.

2.4. Jetting of Applicative Fluids

Jetting of ink solutions of industrial interest was demonstrated using Clevios PH1000 and a suspension of ZnO nanoparticles. Clevios PH1000 is a PEDOT:PSS (3,4-polyethylene-dioxythiophene) water-based solution, provided by Heraeus. It is one of the best hole transport conductive polymers with a very broad range of applications, including new kinds of flexible displays, high-performance electrolytic capacitors, flexible organic solar cells, antistatic and conductive protective layers (ESDs), OLEDs, and printed electronics.[37,38] The ZnO nanoparticle suspension is a water-based mixture, without any additives, provided by Sigma-Aldrich. The suspension contains 20% wt. of zinc oxide nanoparticles with an average diameter of 40 nm. Some noteworthy applications are gas sensors, chemical sensors, biosensors, antimicrobials, cosmetics, storage, optical and electrical devices, solar cells and drug delivery. Concerning the biomedical field, it exhibits important anticancer activity, enhanced by the peculiar electrostatic interaction between the nanoparticles and the cancer cells. This can be further exploited using ZnO nanoparticles as smart-drug carriers, leading to an in situ drug release.[39,40] Finally, it constitutes an ideal model fluid for applications concerning jetting of suspensions such as the ones encountered in the ceramics and glass industry.

To stabilize both inks and reduce satellites, they were diluted with 20% v/v glycerin. ZnO concentrations was adjusted to 10% wt. The addition of glycerin has a beneficial effect in stabilizing the jetting, reducing the satellites and the coffee ring effect (CRE) for the PEDOT:PSS ink. Regarding the latter, the addition of glycerin also increases by orders of magnitude the conductivity of the ink. As a consequence of their dilution and modification with glycerin, the two solutions were characterized to determine their rheological properties prior to jetting characterization (**Figure 8**a). Both the Clevios-based ink and the ZnO nanoparticle suspension showed a clear non-Newtonian pseudoplastic behavior. In the case of PEDOT, which is a polymer, this behavior was expectable. Indeed, many polymers present a shear thinning trend, which is caused by the disentanglement of polymer chains during flow.[41] The pseudoplastic behavior was even more evident in the case of ZnO. Also in this case, shear thinning was expected because many nanoparticle suspensions exhibit it.[42]

All the jetting tests were performed using the PZT_B printhead material with the design PD_A, characterized by bigger geometrical features, especially the nozzle diameter. This helped avoiding nozzle clogging and reducing the shear stresses acting on fluids. This is because the selected inks show a non-Newtonian behavior with shear-thinning features and are prone to generate many satellites, even at low voltages.

As a consequence of their pseudoplastic nature, the viscosity of both applicative inks depends on the shear rate applied. In inkjet printing, different shear rates are applied to the ink when it flows into different zones of the jetting chamber. Normally, low shear rates are experienced by the fluid when it is in the main chamber or in the inlets. High shear stresses can be reached, of the order of 10^4 s^{-1} or even higher, in correspondence with the nozzle, and this condition can dramatically change how the fluid behaves. Due to their pseudoplastic behavior, the two fluids are poorly printable with commonly available printers.

Regarding undiluted Clevios PH1000, the provided datasheet states a viscosity between 15 and 60 cP. By considering the data reported in Figure 8a between 10^2 and 10^4 s^{-1}, diluted Clevios PH1000 was characterized by a viscosity between 34.83 ± 0.34 and 8.58 ± 0.21 cP. Regarding the undiluted ZnO nanoparticles suspension, it has a declared zero-shear-rate viscosity of 30 cP. By considering the data reported in Figure 8a between 10^2 and 10^4 s^{-1}, the diluted ZnO suspension was characterized by a viscosity between 18.38 ± 0.44 and 4.51 ± 0.12 cP. The pseudoplastic characteristic of the fluid can be both a positive and negative factor for inkjet printing: it could help in jetting higher zero-shear-viscosity fluids by exploiting the shear-thinning behavior, but, on the other side, it could cause too many satellites because of the too low viscosity.

Figure 8b shows the results related to the jetting of the GLY-diluted ZnO nanoparticle suspension. The corresponding values for drop velocity and volume are reported in Figure S10, Supporting Information. Despite the curves appearing to be less ideal compared to the ones previously presented, the fluid could be easily jetted and a nonmonotonic trend was observed. It was possible to identify an OPW and an OV, corresponding to 2.3 μs and 34 V. Under these optimal conditions, a drop velocity of 7 m s^{-1} and a drop volume of 21 pL were achieved. The base voltage at which the system started to jet was 26 V. Figure 8c, d shows the results related to the jetting of the GLY-diluted PEDOT:PSS solution. The corresponding values for drop velocity and volume are reported in Figure S11, Supporting Information. As for the ZnO nanoparticle suspension, the curves always showed a nonmonotonic trend. The identified OPW and OV were 2,1 μs and 30 V. Under these conditions, a drop velocity of 7 m s^{-1} and a drop volume of 24 pL were achieved. The base voltage at which the system starts to jet was 27 V.

3. Conclusion

The printhead prototype described in this article successfully jetted highly viscous and non-Newtonian fluids, characterized by Z values significantly lower than 1. Droplets having controllable volumes and speeds were obtained as a function of the printing parameters used. Fluids with viscosities in excess of 200 cP were printed. In general, an increase in viscosity resulted in an increase of both the printing onset potential and satellite onset potential. At constant PZT actuation potential, a viscosity increase resulted in a generalized decrease of droplet speed and kinetic energy. All these aspects have been explained considering the physics of the printing system used and their variations have been linked to secondary ink parameters such as speed of sound and surface tension. In the final part of the article, two

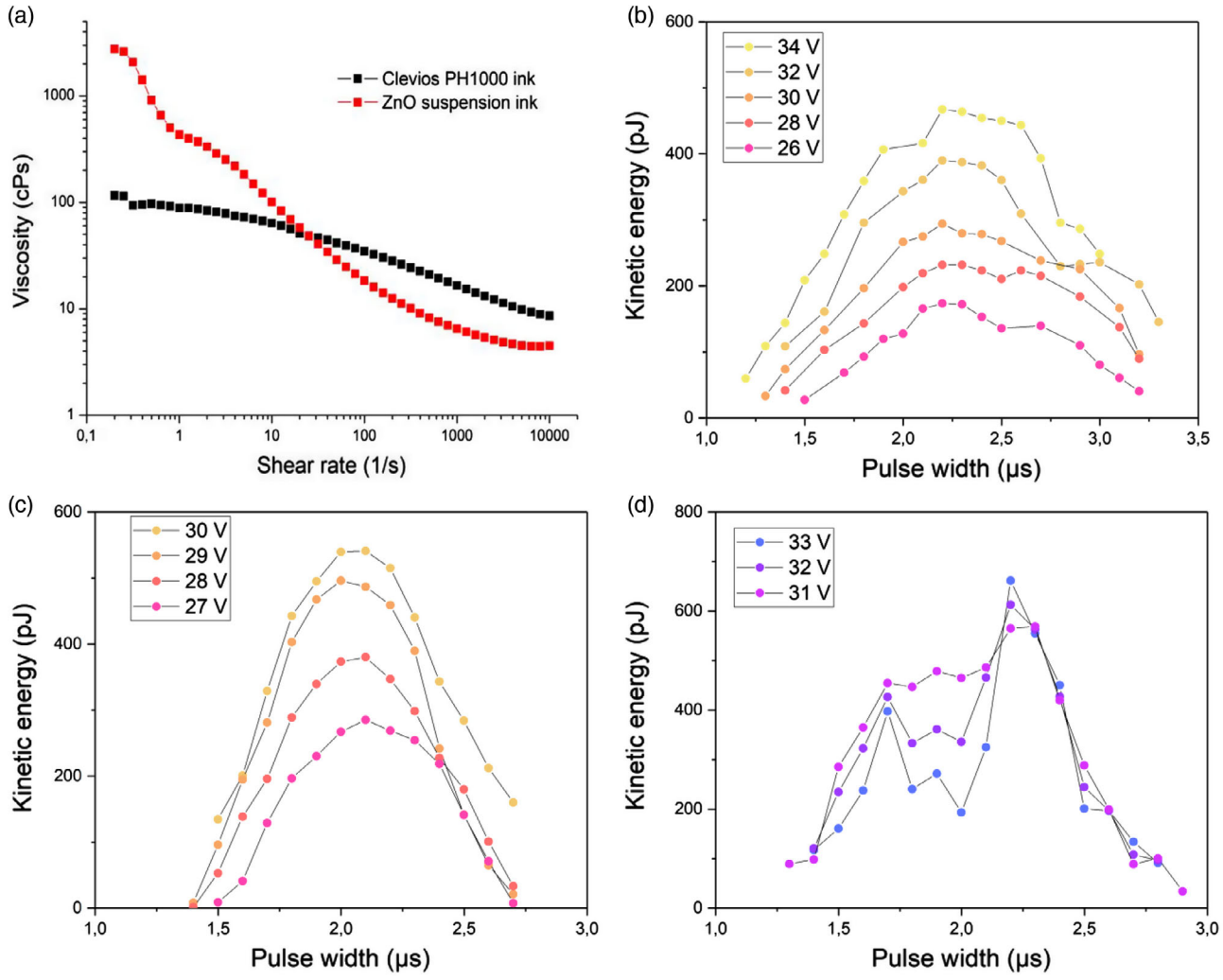

Figure 8. a) Rheological characterization of the Clevios PH1000 ink and of the suspension of ZnO nanoparticles, b) kinetic energy versus pulse width by varying the applied tension for the ZnO suspension jetted through a PD_A printhead design featuring PZT_B material, c) kinetic energy versus pulse width by varying the applied tension up to the onset of satellites for the Clevios PH1000 ink jetted through a PD_A printhead design featuring PZT_B material, and d) kinetic energy versus pulse width by varying the applied tension beyond the onset of satellites for the Clevios PH1000 ink jetted through a PD_A printhead design featuring the PZT_B material.

viscous non-Newtonian pseudoplastic applicative fluids were successfully jetted. The ZnO nanoparticle suspension used suggested possible applications in the jetting of ceramics for applications in sensing or microelectronics. The PEDOT:PSS solution, in contrast, constituted a good example of a concentrated polymer solution, which can potentially find application in the patterning of polymeric layers.

4. Experimental Section

Materials: Ethylene glycol (99,8% purity), glycerin (99% purity), and ZnO nanoparticle suspension (20 wt% in H_2O) were purchased from Sigma-Aldrich. Clevios PH1000 (1–1.3% solid content) was purchased from Heraeus. The explored viscosity range spans from 10 to 300 cP, 200 cP being the maximum viscosity reached during the jetting phase. The physical properties of the water–EG and water–GLY mixtures are available from the literature.[43–48] Consequently, suitable amounts of EG and water were mixed to obtain a 10 cP solution. Analogously, GLY and water were mixed in different proportions to obtain solutions having the following viscosities: 100, 200, 250, and 300 cP.

Die Design and PZT Materials: Figure S1, Supporting Information, details the geometry of the dies used. Two printhead die designs were tested and compared: PD_A and PD_B. These designs are characterized by different internal geometries, such as for the inlet shape, channel cross-section and nozzle diameter. The designs specifications are reported in Table S1, Supporting Information. The dies were designed to support ink recirculation, so each chamber has two inlets. Figure S2, Supporting Information, shows the IR spectroscopy of the two different designs. As shown in Figure S2, Supporting Information, the inlet and nozzle descender shapes are different. For design A, the features are bigger and squared. For design B, the inlets, descender, and nozzles are visibly smaller and rounded. In addition, two PZT material compositions were tested, PZT_A and PZT_B. Both were processed with a sol–gel approach, under the same environmental conditions, but leading to different final compositions. PZT_A has a composition out of the morphotropic phase boundary (MPB), and PZT_B was processed to obtain a MBP-compliant material.

Experimental Setup: The experimental setup involved a programmable waveform generator (Keysight 81150 A), a low-voltage DC generator (Keithley 2230), a high-voltage DC generator (Elind HS), an oscilloscope (Agilent InfiniiVision DSO-X 2024 A), a class-D audio amplifier board, and a JetXpert setup. The goal of the driving equipment was to generate a high-voltage pulsed signal, with an amplitude ranging between 10 and 60 V, which was directly fed to the printhead. A high-voltage DC generator (Elind HS) and a programmable waveform generator (Keysight 81150 A) were used to freely tune and adjust all the parameters related to the pulsed signal. The former provided the requested DC voltage, adjusted by the means of a knob, with a maximum current of 10 A. The latter generated the pulsed waveform, which was tuned by setting the proper frequency, pulse width, and rise and fall times. The pulsed signal, along with the high DC voltage, were fed into the custom class-D audio amplifier. This board, depending on the waveform polarity, acts as a fast–high voltage switch: it can ground the DC signal or let it pass, depending on the shape of the pulsed trigger signal. Rise and fall times of about 80–100 ns can be achieved, leading to a close-to-ideal pulsed signal, compared to the typical pulse widths of about 2 µs. The low-voltage DC generator (Keithley 2230) was used to power the audio amplifier, with a voltage of 5 V and an idle power consumption of 68 mA. The output waveform was directly taken from the audio amplifier and fed into the printhead. The oscilloscope (Agilent InfiniiVision DSO-X 2024 A) was attached to the class-D audio amplifier outputs to measure the effective parameters of the driving waveform. The JetXpert system is a stroboscopic camera (Allied Vision Technologies), synchronized with the trigger signal from the waveform generator. An LED emits the necessary light to freeze the motion of the drops and the printhead is mounted in the working space of the system, just above the stroboscopic line of sight between the two lenses.

Rheological Characterization: The rheological properties of the applicative inks were tested using a rotational rheometer (MCR 302, Anton Paar). All the tests were conducted using a parallel-plate configuration (diameter 25 mm, working gap 1 mm).

Supporting Information

Supporting Information is available from the Wiley Online Library or from the author.

Acknowledgements

The authors would like to thank Lorenzo Bonetti for the rheological characterization.

Open Access Funding provided by Politecnico di Milano within the CRUI-CARE Agreement.

Conflict of Interest

The authors declare no conflict of interest.

Data Availability Statement

The data that support the findings of this study are available from the corresponding author upon reasonable request.

Keywords

drop on demand, high viscosity, inkjet printing, piezoelectric

Received: June 14, 2021
Revised: July 26, 2021
Published online:

[1] M. Singh, H. M. Haverinen, P. Dhagat, G. E. Jabbour, *Adv. Mater.* **2010**, *22*, 673.
[2] B. Derby, *J. Mater. Chem.* **2008**, *18*, 5717.
[3] R. Bernasconi, D. Meroni, A. Aliverti, L. Magagnin, *IEEE Sens. J.* **2020**, *20*, 14024.
[4] J. D. Kim, J. S. Choi, B. S. Kim, Y. Chan Choi, Y. W. Cho, *Polymer* **2010**, *51*, 2147.
[5] S. Kholghi Eshkalak, A. Chinnappan, W. A. D. M. Jayathilaka, M. Khatibzadeh, E. Kowsari, S. Ramakrishna, *Appl. Mater. Today* **2017**, *9*, 372.
[6] E. Tekin, P. J. Smith, U. S. Schubert, *Soft Matter* **2008**, *4*, 703.
[7] V. Fakhfouri, G. Mermoud, J. Kim, A. Martinoli, J. Brugger, *Micro Nanosyst.* **2009**, *1*, 63.
[8] B. jo, A. Lee, K. Ahn, S. Lee, *Korean J. Chem. Eng.* **2009**, *26*, 339.
[9] R. Bernasconi, M. C. Angeli, F. Mantica, D. Carniani, L. Magagnin, *Polymer* **2019**, *185*, 121933.
[10] H. P. Le, *J. Imaging Sci. Technol.* **1998**, *42*, 49.
[11] S.-H. Kang, S. Kim, D. K. Sohn, H. S. Ko, *Phys. Fluids* **2020**, *32*, 022007.
[12] B. Derby, *Annu. Rev. Mater. Res.* **2010**, *40*, 395.
[13] Q. Huang, Y. Zhu, *Adv. Mater. Technol.* **2019**, *4*, 1800546.
[14] J. Choi, Y.-J. Kim, S. Lee, S. U. Son, H. S. Ko, V. D. Nguyen, D. Byun, *Appl. Phys. Lett.* **2008**, *93*, 193508.
[15] A. Endo, J. Akedo, *Synth. Engl. Ed.* **2011**, *4*, 9.
[16] K. E. Paul, W. S. Wong, S. E. Ready, R. A. Street, *Appl. Phys. Lett.* **2003**, *83*, 2070.
[17] L. Nayak, S. Mohanty, S. K. Nayak, A. Ramadoss, *J. Mater. Chem. C* **2019**, *7*, 8771.
[18] Z. Zhou, L. Ruiz Cantu, X. Chen, M. R. Alexander, C. J. Roberts, R. Hague, C. Tuck, D. Irvine, R. Wildman, *Addit. Manuf.* **2019**, *29*, 100792.
[19] P. J. Yunker, T. Still, M. A. Lohr, A. G. Yodh, *Nature* **2011**, *476*, 308.
[20] D. Mampallil, H. B. Eral, *Adv. Colloid Interface Sci.* **2018**, *252*, 38.
[21] P. Delrot, M. A. Modestino, F. Gallaire, D. Psaltis, C. Moser, *Phys. Rev. Appl.* **2016**, *6*, 024003.
[22] H. Yang, Y. He, C. Tuck, R. Wildman, I. Ashcroft, P. Dickens, R. Hague, presented at *Twenty Forth Annual International Solid Freeform Fabrication Symposium—An Additive Manufacturing Conference*, August **2013**, pp.505–513.
[23] Y. Chen, D. Munoz-Martin, M. Morales, C. Molpeceres, E. Sánchez-Cortezon, J. Murillo-Gutierrez, *Phys. Procedia* **2016**, *83*, 204.
[24] M. Makrygianni, A. Milionis, C. Kryou, I. Trantakis, D. Poulikakos, I. Zergioti, *Adv. Mater. Interfaces* **2018**, *5*, 1800440.
[25] T. T. T. Can, T. C. Nguyen, W.-S. Choi, *Adv. Eng. Mater.* **2020**, *22*, 1901384.
[26] N. Jackson, W. Voit, R. Trip, A. Condie, X. Plc, presented at *NIP & Digital Fabrication Conference*, September **2019**, pp.89–93.
[27] B.-J. de Gans, P. C. Duineveld, U. S. Schubert, *Adv. Mater.* **2004**, *16*, 203.
[28] N. Reis, B. Derby, *MRS Proc.* **2000**, *625*, 117.
[29] D. Jang, D. Kim, J. Moon, *Langmuir* **2009**, *25*, 2629.
[30] A. Lee, K. Sudau, K. H. Ahn, S. J. Lee, N. Willenbacher, *Ind. Eng. Chem. Res.* **2012**, *51*, 13195.
[31] K. A. Mann, S. Deutsch, J. M. Tarbell, D. B. Geselowitz, G. Rosenberg, W. S. Pierce, *J. Biomech. Eng.* **1987**, *109*, 139.
[32] S. D. Hoath, W.-K. Hsiao, S. Jung, G. D. Martin, I. M. Hutchings, N. F. Morrison, O. G. Harlen, *J. Imaging Sci. Technol.* **2013**, *57*, 10503.

[33] K.-S. Kwon, *J. Micromech. Microeng.* **2010**, *20*, 115005.
[34] F. Marangon, W. K. Hsiao, G. Brenn, C. Planchette, in *Proc. of the 29th Conf. on Liquid Atomization and Spray Systems*, September **2019**.
[35] G. Fan, W. Lu, X. Wang, F. Liang, *Appl. Phys. Lett.* **2007**, *91*, 4.
[36] R. S. Solanki, S. K. Mishra, C. Moriyoshi, Y. Kuroiwa, I. Ishii, T. Suzuki, D. Pandey, (Preprint) arXiv:1703.02259 (submitted: March 2017).
[37] X. Fan, W. Nie, H. Tsai, N. Wang, H. Huang, Y. Cheng, R. Wen, L. Ma, F. Yan, Y. Xia, *Adv. Sci.* **2019**, *6*, 1900813.
[38] S. Lee, *J. Nanosci. Nanotechnol.* **2016**, *16*, 2880.
[39] U. Ojha, S. Das, S. Chakraborty, *J. Mater. Sci. Eng.* **2010**, *4*, 7.
[40] P. K. Mishra, H. Mishra, A. Ekielski, S. Talegaonkar, B. Vaidya, *Drug Discov. Today* **2017**, *22*, 1825.
[41] K. S. Sorbie, in *Polym.-Improv. Oil Recovery* (Ed.: K. S. Sorbie), Springer Netherlands, Dordrecht, **1991**, pp. 37–82.
[42] M. Adil, H. M. Zaid, L. K. Chuan, N. R. A. Latiff, *Energy Fuels* **2016**, *30*, 6169.
[43] D. Bohne, S. Fischer, E. Obermeier, *Berichte Bunsenges. Für Phys. Chem.* **1984**, *88*, 739.
[44] H. J. Hebert, *J. Acoust. Soc. Am.* **1971**, *49*, 930.
[45] T. Sun, A. S. Teja, *J. Chem. Eng. Data* **2003**, *48*, 198.
[46] N.-S. Cheng, *Ind. Eng. Chem. Res.* **2008**, *47*, 3285.
[47] K. Takamura, H. Fischer, N. R. Morrow, *J. Pet. Sci. Eng.* **2012**, *98–99*, 50.
[48] C. M. Romero, M. S. Paéz, *Phys. Chem. Liq.* **2006**, *44*, 61.